QC-06-054

Testing and Modeling of Underfloor Air Supply Plenums

Hui Jin, PhD
Member ASHRAE

Fred S. Bauman, PE
Member ASHRAE

Tom Webster, PE
Member ASHRAE

ABSTRACT

The use of an underfloor plenum to deliver conditioned air directly into the occupied zone of a building is one of the key features that distinguish underfloor air distribution systems from conventional ducted overhead systems. This paper describes the development, validation, and application of a computational fluid dynamics (CFD) model for predicting the airflow and thermal performance of underfloor air supply plenums. To provide validation data for comparison with the CFD model, a series of experiments in a full-scale underfloor plenum test facility were carried out. The results of the experiments and comparison with the model predictions are described for the major variables, including plenum airflow patterns and velocities, plenum air temperature distributions, and heat exchange between the exposed concrete slab, the underside of the raised floor panels, and the supply air as it flows through the plenum. The validated CFD model was used to perform additional simulations to investigate the impact of plenum inlet design parameters (location and airflow direction and velocity) on the plenum heat gain and temperature distribution. Implications for the design and operation of underfloor air supply plenums are discussed.

INTRODUCTION

Underfloor air distribution (UFAD) offers several potential advantages over conventional overhead systems. However, barriers exist to widespread adoption of UFAD since it is a relatively new and unfamiliar technology. One of the major technical challenges is to precisely quantify the air movement and heat transfer behavior taking place in the underfloor air supply plenum. Cool supply air flowing through the underfloor plenum in a multi-story building is exposed to heat gain from both the concrete slab (conducted from the warm return air on the adjacent floor below the slab) and the raised floor panels (conducted from the warmer room above). The magnitude of this heat gain can be quite high, resulting in undesirable loss of control of the supply air temperature from the plenum into the occupied space, sometimes referred to as *thermal decay* (Webster et al. 2002; Bauman 2003; CBE 2005). To date, evidence from completed projects indicates that excessive thermal decay can be a problem.

Due to the large number of possible plenum configurations (size, shape, number and location of plenum inlets, etc.) encountered in practice, along with the complexity of the airflow and thermal behavior, it is desirable to develop a validated mathematical model of underfloor air supply plenums. This was the major objective of the research described in this paper. To characterize the major variables that must be accommodated by the underfloor plenum model, experiments were carried out in a full-scale underfloor plenum test facility. A range of practical design and operating parameters that can affect the performance of UFAD systems were investigated. The fundamental heat transfer processes and parameters that were the focus of these experiments include plenum airflow pattern and velocity, plenum air temperature distribution, and total heat exchange between the exposed concrete structural slab, the underside of the raised floor, and the supply air as it flows through the underfloor plenum. Experimental data were collected for comparison with and validation of the numerical calculations. A computational fluid dynamics (CFD) model using a commercial software package was developed to match the full-scale test facility and finely tuned to replicate the experimental measurements. In order to demonstrate the capabilities of the validated CFD

Hui Jin, **Fred S. Bauman**, and **Tom Webster** are research specialists at the Center for the Built Environment, University of California, Berkeley, California.

plenum model, it was used to conduct a series of sensitivity studies on selected design parameters.

A review of the literature yields few references related to modeling of underfloor air supply plenums. Fujita and Tomiie (1999) developed a model to estimate the convective heat transfer coefficients between the plenum air and the concrete slab below and the underside of the raised floor panels above. However, this approach did not address the variation of the heat transfer coefficient at different locations of the plenum (due to differences in velocity) or how to extend the model to plenums with different design parameters, such as shape, size, and inlet velocities. Nagase et al. (1995) measured the cooling load of a UFAD test chamber and compared that with the room extraction rate. Data showed that the cooling load was substantially greater than the room extraction rate. The agreement was improved with an insulated access floor, which indicated that the discrepancy might be due to the heat transfer from the room into the underfloor supply plenum through the floor panel.

In this paper we (1) describe the underfloor air supply plenum test facility and the accompanying data acquisition system, (2) describe the CFD plenum model, (3) describe the validation of the CFD model by comparison with the experimental data, and (4) present a sample sensitivity analysis using the validated CFD model.

EXPERIMENTAL FACILITY

Underfloor Plenum

The underfloor air supply plenum test facility was installed in December 2000 in a university warehouse with an exposed concrete slab floor. Figure 1 shows plan and section views of the plenum structure. The plenum is 22 × 74 ft (6.7 × 22.6 m) and 1 ft (0.305 m) high. The raised floor system was constructed from commercially available floor panels and included 16 variable-air-volume (VAV) floor diffusers. The plenum occupies three bays defined by 25 ft (7.6 m) on center columns in the warehouse, with one edge bordering an exterior wall. A heating, ventilating, and air-conditioning (HVAC) system delivers supply air at a controlled temperature and volume into the underfloor plenum. The HVAC system has 2,330 cfm (1100 L^3/s) as the maximum supply airflow and 55°F–90°F (13°C–32°C) as the operable temperature control. The plenum inlet was installed at the middle of the side wall next to the HVAC system. In order to reduce the cost of instrumentation and CFD modeling, the plenum was afterwards divided into two parts by a plastic partition, depicted in Figure 1 by the dashed line. Testing and modeling were accomplished on the left section of the plenum (Figure 1). The plenum section is 22 × 48 ft (6.7 × 14.6 m), which is approximately two-thirds of the original size. As shown in Figure 1, ten diffusers fall into this part of the plenum. The gaps between the floor panels and plenum edges were taped to eliminate air leakage for purposes of comparison with the CFD model predictions. The floor panels are 2 × 2 ft × 1.3 in. (0.6 × 0.6 × 0.033 m) constructed from a welded steel outer shell filled with lightweight cementitious material. The thermal conductivity of a bare panel is 1.359 Btu·in./h·ft^2·°F (0.196 W/m·K), and that of a panel with carpet tiles is 1.002 Btu·in./h·ft^2·°F (0.144 W/m·K). The plenum is built on a structural concrete slab 10 in. (0.254 m) thick with thermal conductivity of 0.54 Btu/h·ft·°F (0.93 W/m·K).

Plenum Inlet Configurations

Preliminary calculations showed that the inlet configuration can have a significant impact on the plenum air temperature variation and heat gain. Two different inlet configurations were installed and tested to provide validation data for the

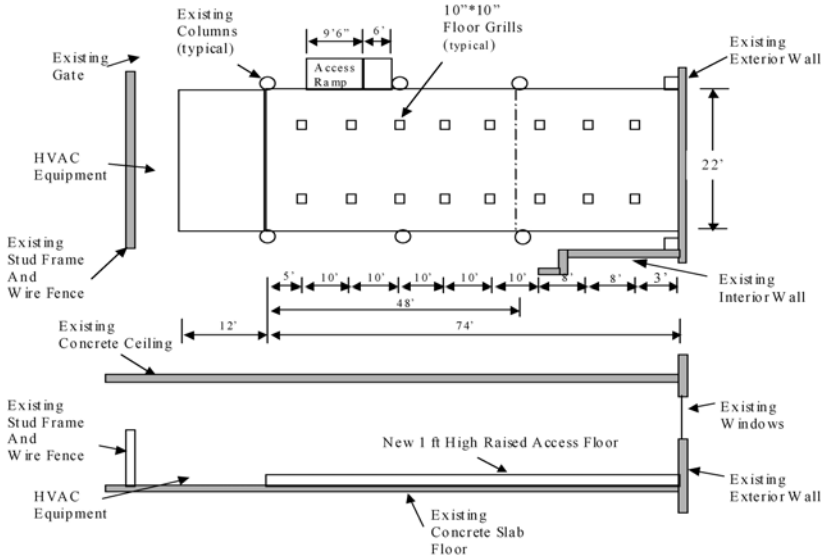

Figure 1 *Plan and section views of underfloor air supply plenum test facility.*

CFD model. They are one single focused jet and two jets, which is a simplified version of an inlet vane configuration that produces multiple jets. Schematic diagrams of the single focused jet and inlet vanes/two jets inlet configurations are shown in Figure 2.

Single Focused Jet. Flow straighteners and filter material are used to establish relatively uniform inlet airflow conditions, allowing more precise specification of the inlet conditions within the CFD model. It is noted that the direction of the single focused jet is not perpendicular to the short side of the plenum. The plenum inlet is located at the middle of the short side of the plenum. Thus, the geometry may be looked upon as simply symmetric. However, a symmetric geometry does not necessarily ensure a symmetric flow pattern. First, it is challenging to obtain a completely uniform inlet velocity throughout the cross-sectional area of the inlet. Second, due to the random and asymmetric nature of the turbulent flow, the airflow for the given single focused inlet jet configuration and plenum shape will not produce a perfectly symmetric pattern. In addition, information about an unrealistically symmetric flow pattern may not be normally useful in practice. In order to bypass the complexity introduced by the symmetric geometry, the direction of the inlet jet was turned to one side at a small angle from normal.

Inlet Vanes/Two Jets. Inlet vanes are one approach to spreading out and slowing down the inlet airflow. In this case, the inlet airflow can be represented experimentally as a collection of individual jets. Initial experiments and calculations indicated that the airflow pattern and air temperature distribution were very sensitive to the direction and momentum of each inlet jet. For the sake of simplicity, two jets were fabricated to investigate the influence of the inlet vanes configuration.

Measurement Setup

Type-T thermocouples and a modular data acquisition and control system were installed to monitor air temperatures at the plenum inlet, floor diffusers, and selected locations inside the plenum. Four inch (100 mm) deep holes were drilled at selected locations of the slab to obtain vertical slab temperature measurements at 1 in. (25 mm) intervals. Since there is no control of the heat transfer from under the slab (a loading dock is located on the warehouse floor below), the vertical temperature profile of the slab is very useful to implicitly derive the boundary conditions for the CFD simulation. Space air temperatures were measured just above the raised floor panels to obtain the boundary conditions above the plenum. If the heat transfer through the sidewalls of the plenum is neglected, the total heat gain into the plenum is the sum of heat transfer through the floor panels and concrete slab. In addition to convective heat transfer from the room air to the raised floor panels, recent research findings have shown that the radiative heat transfer from the warm ceiling (especially in a stratified UFAD space) to the floor could account for the majority of the heat gain through the floor panels into the plenum (Bauman et al. 2006). Therefore, the ceiling temperature needs to be considered an important part of the specification of the boundary conditions above the plenum. It was measured using an infrared temperature sensor.

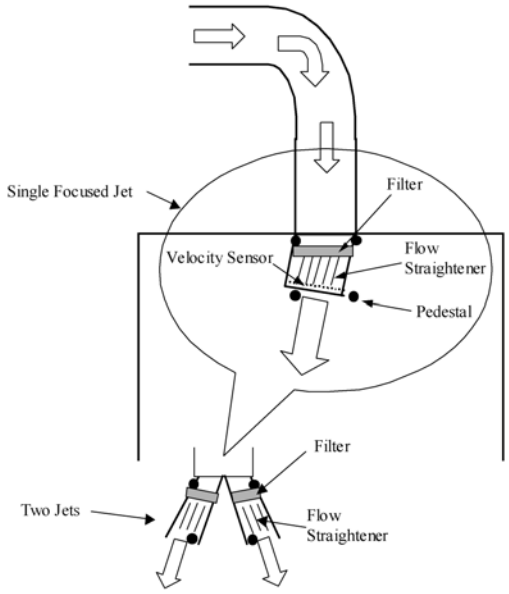

Figure 2 *Schematic of the single focused jet and inlet vanes/two jets inlet configurations.*

The plenum inlet air velocity is measured by a low air velocity and air temperature measuring system with a cylindrical (directional) probe. The readings are then converted into the plenum inlet air supply volume by applying the cross-sectional area of the inlet opening. The air velocities at selected locations inside the plenum are measured by the same system, with a spherical (omni-directional) probe. The cylindrical and spherical probes provide the measurement range of 0.15 to 10 m/s (30 to 2,000 ft/min) and 0.05 to 5 m/s (10 to 1,000 ft/min), respectively. Both probes have the accuracy of ±3% of the readings. The voltage outputs of the anemometers are connected to the existing data acquisition system.

For the slab and floor heat flux measurements, a heat flux transducer was used. The thermal flux meter is a solid-state, flat-plate transducer designed to measure heat flux directly. The meter is placed on any surface through which the heat flow is to be measured. The heat flux meter has an accuracy of 1% of the reading. Four flux meters were attached to selected locations at the top surface of the slab and floor panel. The voltage outputs of the flux meters are also connected to the existing data acquisition system.

Figure 3 shows the locations selected for the air temperature and velocity and slab/floor heat flux sensors. Based on preliminary experimental observation and CFD simulation, the measurements at these key locations were used to characterize the predominant airflow pattern, air temperature distribution, and heat transfer from above and below the plenum.

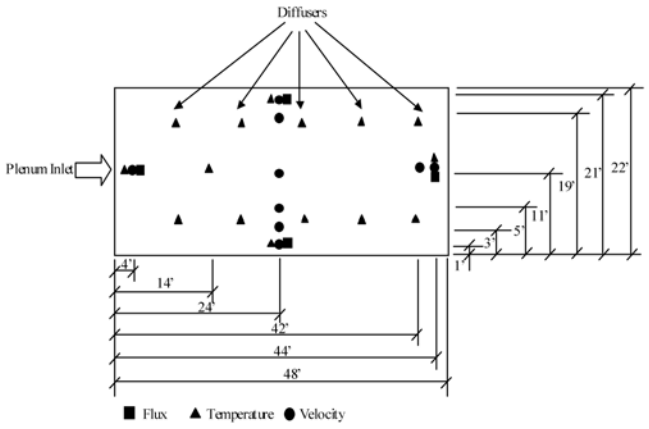

Figure 3 *Locations of the sensors for data acquisition system.*

Experimental data collected under steady-state conditions for the two different inlet configurations were used to validate the CFD plenum model described below.

DESCRIPTION OF THE CFD MODEL

The use of CFD modeling to solve flow and heat transfer problems is increasing within the HVAC industry. CFD programs provide a detailed analysis of the thermal fluid phenomena, producing simulation results that include qualitative values, such as airflow pattern, and quantitative values, such as air velocity, temperature, turbulence kinetic energy, Reynolds stress, and surface heat flux. These parameters reported by the CFD code can be used for comparison with the experimental data. Generally speaking, air velocity and temperature can be simulated and measured with greater accuracy than the other parameters in both CFD and experimental applications. Since determining the overall heat gain into the plenum is one of the primary objectives of this ongoing research, heat flux was another important parameter involved in the comparison between the CFD simulation and experiment.

Governing Equations

The partial differential equations solved by the CFD code are the unsteady Navier-Stokes equations in their conservation forms. The instantaneous equations of mass, momentum, and energy conservation can be written as follows.

The continuity equation

$$\frac{\partial \rho}{\partial t} + \nabla \cdot (\rho U) = 0 \qquad (1)$$

where

ρ = density, kg/m^3 (lb/ft^3)

U = velocity vector, m/s (ft/min)

The momentum equation

$$\frac{\partial \rho U}{\partial t} + \nabla \cdot (\rho U \times U) = \nabla \cdot \{-p\delta + \mu[\nabla U + (\nabla U)^T]\} + S_M \qquad (2)$$

where

μ = dynamic viscosity, mPa·s (centipoise)

S_M = momentum source, kg/m^2·s^2 (lb/ft^2·min^2)

The energy equation

When the contribution of the kinetic energy to the total energy can be neglected,

$$\frac{\partial \rho h}{\partial t} + \nabla \cdot (\rho U h) = \nabla \cdot (\lambda \nabla T) + S_E , \qquad (3)$$

where

h = specific static enthalpy, J/kg (ft·lb$_f$/lb);

λ = thermal conductivity, W/m·K (Btu/h·ft·°F); and

S_E = energy source, kg/m·s^3 (lb/ft·min^3).

CFD Models, Auxiliary Heat Transfer, and Flow Models

The turbulence model chosen for the simulation is a standard k-ε model (Launder and Spalding 1974). The k-ε turbulence model is a commonly used model and is suitable for a wide range of applications. As one of the most prominent turbulence models, it has been implemented in most general purpose CFD codes and is considered the industry standard model. Distinguished from typical indoor airflow, which is a mixed convection, the flow in the plenum is generally forced convection flow due to the relatively high velocity and the existence of pedestals as the cause of turbulence throughout the entire domain. The comparison between the experimental data and model predictions discussed in the following sections shows that the k-ε turbulence model can be used with acceptable accuracy.

Depending on the simulation, five heat transfer model options are possible: none, isothermal, thermal energy, total energy, and fluid dependent. The heat transfer model selected for the simulation is the thermal energy model. The thermal energy model neglects high-speed energy effects and is therefore suitable for low-speed flow applications. The heat transfer model is used to predict the plenum heat gain and air temperature variation in the plenum.

Boundary Conditions

The dimensions of the plenum inlet were 10.7 × 24 in. (0.272 × 0.6096 m) and the measured inlet air velocity was 900 fpm (4.5 m/s) for both experiments. The plenum outlet boundary condition is set to zero relative static pressure. Since the plenum is only 1 ft (0.305 m) high, the area of the plenum sidewalls compared with those of the floor and slab is relatively small. Hence, heat transfer through the sidewalls is neglected and the thermal boundary condition at the sidewalls is set to be adiabatic. The heat gain is therefore assumed to be only from

the top and bottom surfaces of the plenum. It is noted that previous research has shown that the radiation from the ceiling of a stratified UFAD space is the dominant driver for the rate of heat transfer through the top surface (raised floor panels) of the plenum (Bauman et al. 2006).

More details about the boundary conditions used for the CFD simulations are depicted in Figure 4. The boundary conditions above the plenum include ceiling temperature $T_{ceiling}$, ceiling emissivity e, and view factor from ceiling to the top surface of the raised floor F. The view factor is assumed to be 1.0 since there were no obstructions (e.g., furniture) in the warehouse to block the thermal radiation from the ceiling to the floor. The boundary conditions under the plenum include air temperature T_{air} and convection coefficient h_c. The boundary conditions at the plenum inlet include the inlet temperature T_{in}, airflow volume V, and inlet velocity v.

It should be clarified that this experiment was not an effort to duplicate any practical operating conditions in a real UFAD system. This plenum was installed in a warehouse where there was no control of the thermal conditions above and below the plenum. Hence, a relatively low plenum supply air temperature was maintained to establish a substantial temperature difference between the plenum and its surroundings.

Source Term: Resistance of Pedestals

Preliminary comparisons showed that measured velocities were substantially lower than the CFD predictions when the resistance of the pedestals was neglected. There were two approaches available for representing the resistance of the pedestals in the CFD model.

1. Actually building the pedestals into the geometry of the CFD model. This approach generally ends up with a huge mesh size due to the resolution required between the pedestals. Hence, it requires a much more powerful computer than what is commonly available. Computation time may also be extended. In addition, building the geometry can be very labor intensive.

2. Adding a resistance to the fluid domain as a source term in the governing equation to represent the resistance caused by the pedestals. Since the pedestals are uniformly distributed throughout the plenum, this approach was chosen for this CFD model due to its simplicity, efficiency, and low requirement for hardware (i.e., memory and CPU speed).

In the CFD plenum model, the resistance of the pedestals is represented by linear and quadratic resistance coefficients,

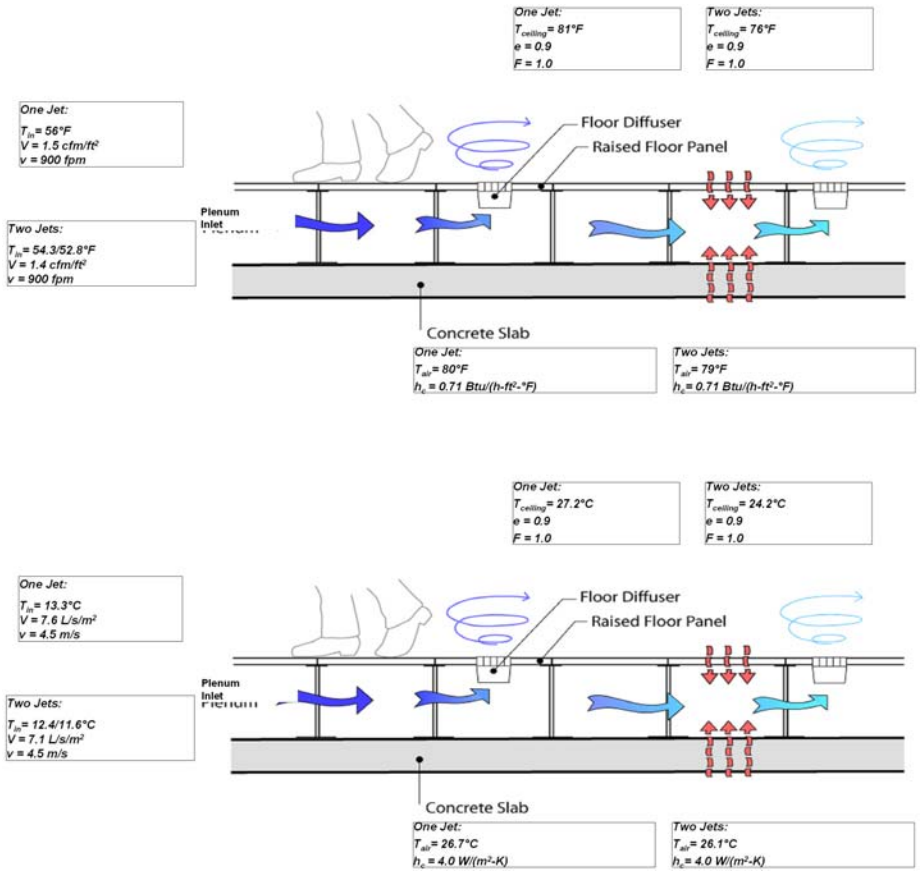

Figure 4 *Boundary conditions of the CFD simulation for the single focused jet and inlet vanes/two jets inlet configurations (top, I-P; bottom, SI).*

C_{R1} and C_{R2}. An isotropic momentum source may be formulated using the generalized form of Darcy's law,

$$S_M = -C_{R1}U_i - C_{R2}|U|U_i\,, \tag{4}$$

where S_M is the momentum source term, kg/m^2·s^2 (lb/ft^2·min^2), and U_i is the velocity, m/s (ft/min). The momentum source term S_M is incorporated into Equation 2 to solve the effect of the resistance of the pedestals on the airflow velocity in the plenum.

Numerical Methods

Parameters for the grid size and quality, such as global element scale factor and global element seed size, were set. The rest of the discretization process is accomplished automatically by the CFD code. Auto time step was selected. This option uses an internally calculated physical time step size based on the specified boundary conditions, initial guesses, and geometry of the domain. It does not require prior knowledge of the approximate time step size for the particular problem.

The numerical scheme was set to high resolution. With this setting, the blend factor values vary throughout the domain based on the local solution field. In flow regions with slow-changing gradients, the blend factor will be close to 1.0 for accuracy. In areas where the gradients change sharply, the blend factor will be closer to 0.0 to prevent over- and underestimates and to maintain robustness.

COMPARISON OF MODEL PREDICTIONS WITH EXPERIMENTAL DATA

The comparison has been based on a steady-state simulation. Since the test facility does not have control of the thermal conditions surrounding the plenum (e.g., the space above and floor below the plenum), it is impractical to obtain the experimental data under complete steady-state conditions. However, due to the fact that the thermal conditions in the large warehouse building containing the test facility and its accompanying systems usually are quite stable and do not experience rapid changes, data collected from quasi-steady-state conditions are acceptable for use in the comparison with theoretical calculations. In the experiment, we delivered a constant temperature and volume of air for at least 72 hours before taking measurements. All of the transient behaviors were minimized after such a relatively long time. Data showed that the variation of temperature and heat flux was negligible during the short period of time (typically 15 minutes) used for the data collection period.

Generally, the comparison of CFD results with the experimental data is the most important part of the reporting process for an indoor-environment CFD analysis. The quantitative comparison between CFD predictions and experimental data includes temperature at each diffuser plus air velocity and slab heat flux at selected locations in the plenum. These data were directly measured in the experiment. The plenum heat gain was calculated based on the measured inlet/outlet temperature difference (where the outlet temperature represents the average of all measured diffuser temperatures) in combination with the airflow volume in the experiment. It can also be computed from CFD results using the same approach. In addition, the heat transfer into the plenum from above the floor and under the slab is obtained from the CFD results. It can be compared against the heat gain into the plenum using the above-described temperature and air volume approach in order to check the convergence of the CFD calculations.

Airflow Pattern

The first step is as simple as a smoke visualization that gives a qualitative comparison for the airflow pattern in the plenum. Figure 5 shows the streamline plots for the single focused jet inlet configuration. The airflow pattern for this case was also investigated using smoke visualization in the test facility. In Figure 5, a big recirculation originating at the plenum inlet and defined by the dimensions of the plenum is observed. The CFD-computed flow pattern agrees very well with that of the smoke visualization. It is noted that the nonuniformity of the air temperatures at diffusers can be clearly explained by this circulation flow pattern. For the two-jet inlet configuration, the big circulation is broken into two relatively small circulations. The shape of the plenum and locations of the inlet and diffusers allow each of the two jets to serve half of the plenum area and diffusers separately in this case. The two jets enter into the plenum from one of the short sides, turn toward the long sides, and flow along these long edges separately until reaching the opposing short side of the plenum. When the two jets reach the far end, they turn around, meeting each other near the midpoint of the far side, and flow back toward the plenum inlet through the central region of the plenum, creating two similarly sized recirculation patterns having the full length of the plenum but only half the width.

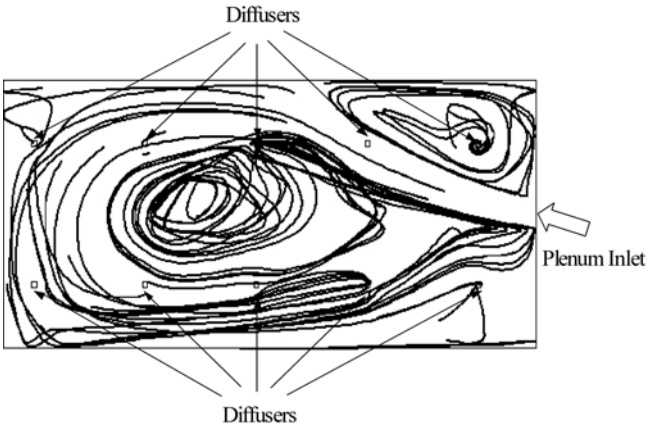

Figure 5 *CFD-simulated airflow pattern of the single focused jet inlet configuration.*

Air Velocity

Figures 6 and 7 present contour plots of the predicted velocity distributions at mid-height of the plenum for the focused jet and two-jet inlet configurations, respectively. Each number on the contour plot represents the average air velocity over the indicated area. In addition, the measured and computed air velocities at selected measurement locations in the plenum are shown. The measured velocities agree quite well with the experimental data. The velocity plot also agrees well with the airflow pattern observed through the use of smoke visualization. Due to the resistance offered by the pedestals, the air velocity decreases so fast that the magnitude of the velocity over most of the area of the plenum is lower than 180 ft/min (0.91 m/s). Hence, it may be reasonable to assume that the overall convective heat transfer coefficient inside the plenum is fairly close to that of natural convection.

Temperatures at Diffusers

Figure 8 presents a contour plot of the predicted temperature distribution at mid-height of the plenum for the focused jet inlet configuration. Each number on the contour plot represents the average air temperature over the indicated area. In addition, the measured and computed temperatures at each of the ten diffusers are shown. Figure 9 presents a comparison of the measured and predicted diffuser temperatures in numerical order for this same inlet configuration. For the focused jet case, the difference between the highest and lowest diffuser temperatures is approximately 10°F (5.6°C). It is observed that diffuser #2 (located within the inlet jet depicted in Figure 8 by the lightest shade) has the lowest temperature, and one of the diffusers located closest to the plenum inlet (#6) has the highest. The flow pattern shown in Figure 5 helps to explain this result. The overall plenum temperature plot in Figure 8 is consistent with the flow pattern. The diffuser that has the lowest temperature is the first one directly impacted by the inlet jet. The diffuser that has the highest temperature is the last one impacted by the expanded airflow pattern, having traveled to the far end of the plenum before recirculating back to the nearby diffuser. This analysis helps to explain observations made in many underfloor supply plenum applications. The diffusers closest to the plenum inlet do not necessarily have the lowest temperatures. The temperature rise depends upon the distance that the inlet air travels before reaching the particular diffuser. Due to the complexity of the airflow pattern

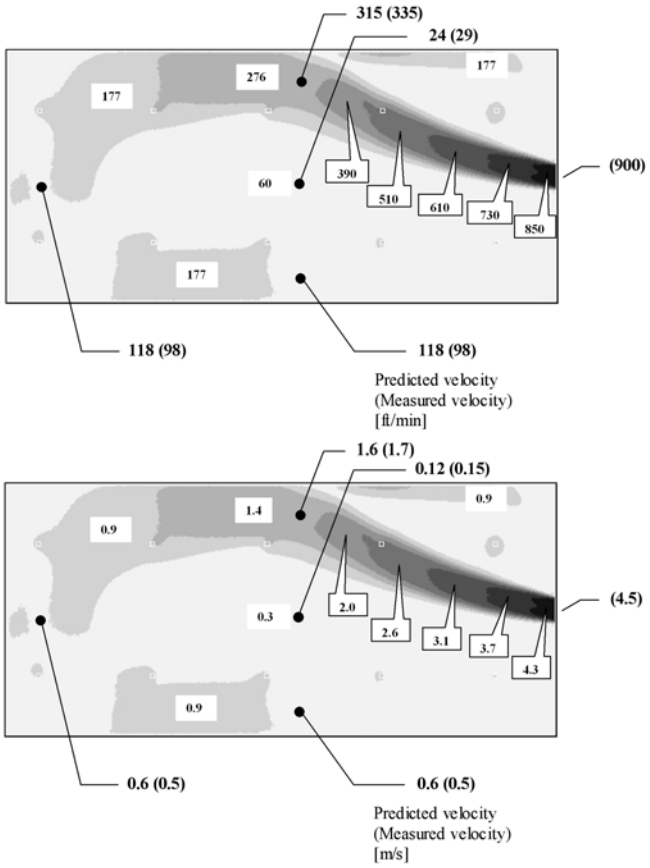

Figure 6 *Comparison of measured and CFD-predicted plenum air velocities for single focused jet inlet configuration (top, I-P; bottom, SI).*

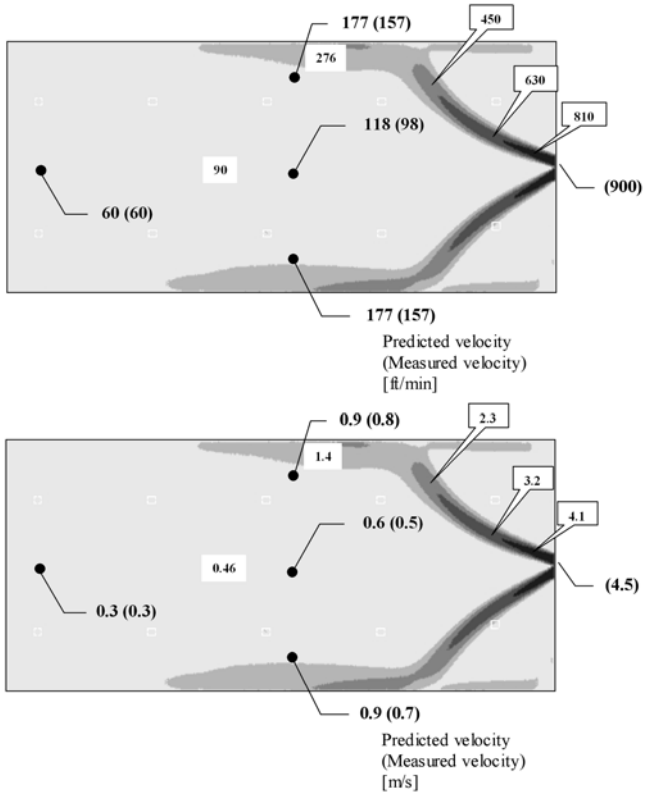

Figure 7 *Comparison of measured and CFD-predicted plenum air velocities for inlet vanes/two jets inlet configuration (top, I-P; bottom, SI).*

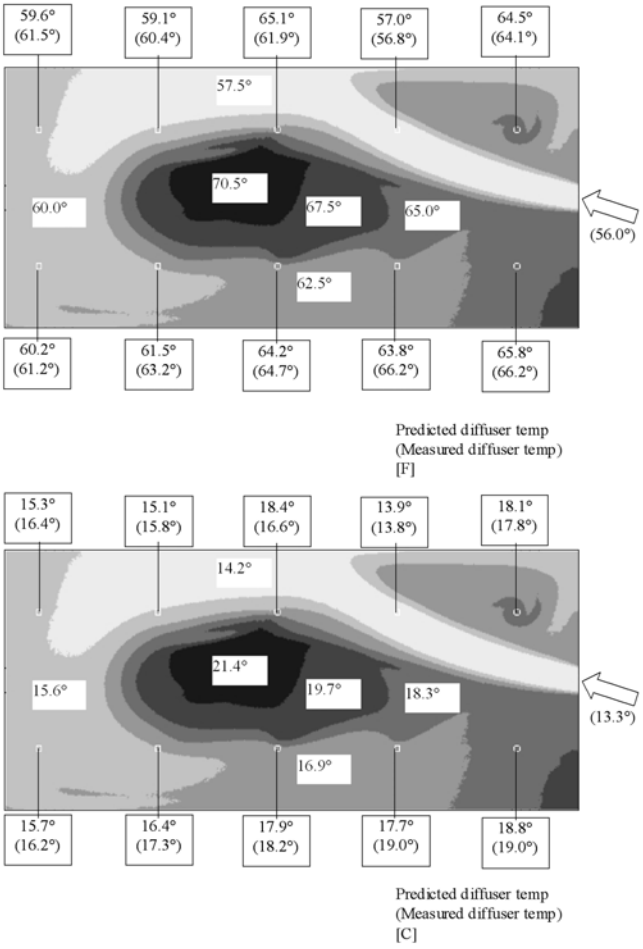

Figure 8 *Comparison of measured and CFD-predicted diffuser temperatures for single focused jet inlet configuration (top, I-P; bottom, SI).*

for a given plenum shape and inlet configuration, the traveled distance is not necessarily the same as the geometric distance between the inlet and diffuser under many conditions.

Figure 10 presents a contour plot of the predicted temperature distribution at mid-height of the plenum for the two-jet inlet configuration. Each number on the contour plot represents the average air temperature over the indicated area. In addition, the measured and computed temperatures at each of the ten diffusers are shown. Figure 11 presents a comparison of the measured and predicted diffuser temperatures in numerical order for this same inlet configuration. For the two-jet inlet configuration, the difference between the highest and lowest temperatures is less than 5°F (2.8°C). As discussed earlier, the flow pattern in this case allows the average distance that the air travels before leaving each diffuser to be shorter than in the single-jet case. As a result, the nonuniformity of the diffuser air temperatures for this flow pattern is greatly improved.

Table 1 presents a comparison of the nonuniformity of the diffuser temperatures between the single focused jet and two-jet inlet configurations. In particular, the standard deviation

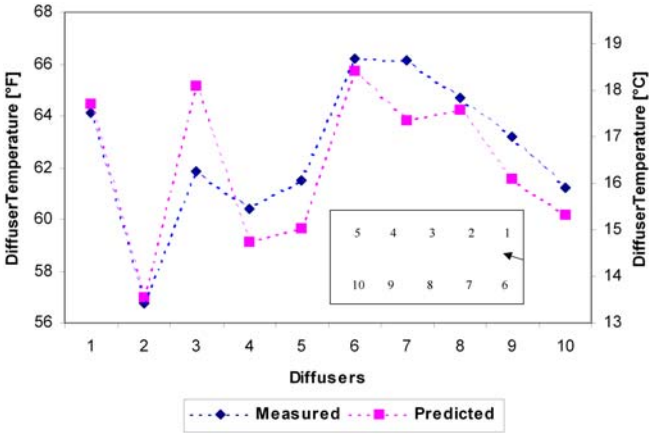

Figure 9 *Comparison of measured and CFD-predicted diffuser temperatures for single focused jet inlet configuration.*

calculation indicates that the two-jet inlet configuration provides more evenly distributed diffuser temperatures throughout the entire plenum.

Slab Heat Flux

The experiments also measured the slab surface heat flux at selected locations. Results indicate that the heat flux has its highest magnitude at locations closest to the inlet, where the highest velocities are observed. When the airflow travels farther into the plenum and slows down, the heat flux decreases accordingly. It is commonly recognized that the convective heat transfer coefficient decreases as velocity decreases. Meanwhile, the temperature difference between the air in the plenum and its boundaries becomes smaller as the plenum air temperature rises. Therefore, among the four selected measurement locations shown in Figure 3, the highest heat flux takes place at the plenum inlet and the smallest heat flux is observed at the location where the velocity is the lowest and the distance the airflow has traveled is the longest. Table 2 shows a comparison of the total heat gain of the plenum between experiment and CFD predictions. Although the test facility does not allow the split of total heat gain into heat transfer through the floor and concrete slab, the CFD model is capable of providing this relatively detailed information. Agreement for the total heat gain into the plenum is found to be within 7% for the single focused jet inlet configuration and within 5% for the two-jet inlet configuration.

DISCUSSION OF RESULTS

While experimental testing has been conducted successfully using a full-scale test facility, the CFD modeling and simulation of the underfloor supply plenum represents a relatively speedy and economical alternative to experimental studies. The CFD analysis can incorporate the actual details of the geometry, material properties, and boundary conditions to

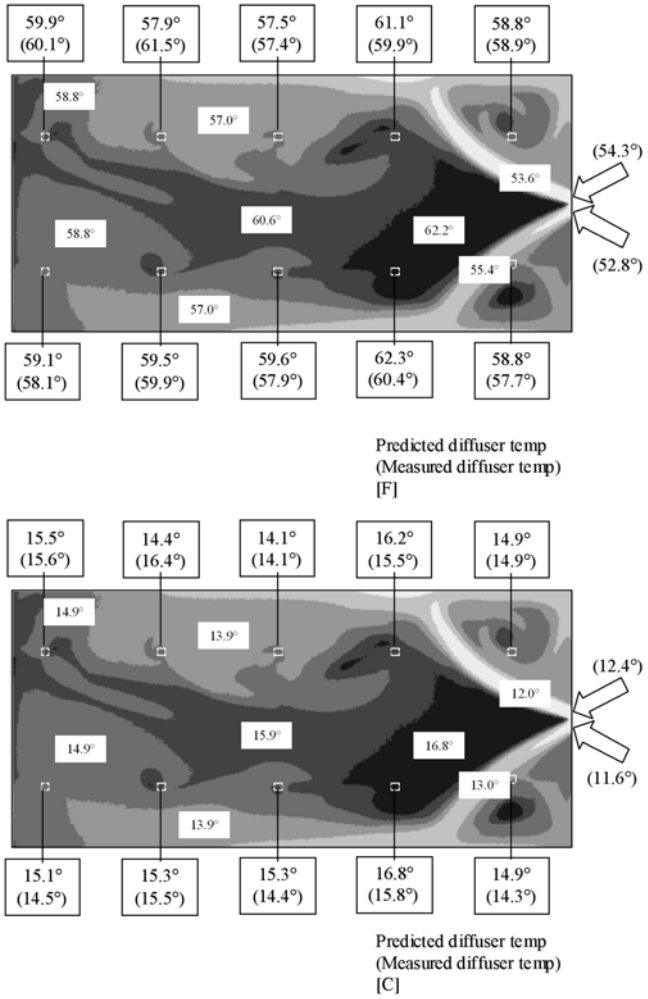

Figure 10 *Comparison of measured and CFD-predicted diffuser temperatures for inlet vanes/two jets inlet configuration (top, I-P; bottom, SI).*

produce complete and detailed information about the distribution of temperature, velocities, etc. In order to validate the CFD model, experimental testing is necessary. On the other hand, the CFD prediction has been used to plan and design the experiment, to significantly reduce the amount of experimentation, and to supplement and enrich the experimental results.

CFD predictions show that the directions of airflow at the inlet of the plenum play an important role in the formation of the flow patterns. As a result of different airflow patterns, the temperature distribution, heat flux distribution, and total heat transfer may vary significantly. In order to carefully validate the CFD model, experiments were conducted for two different plenum inlet configurations: one single focused jet and two separated jets. The boundary and test conditions for these two experiments were replicated in the CFD model simulation. The CFD model was refined progressively based on comparison with the full-scale testing data. The comparison between the final results of the model calculation and test data demonstrates that the CFD model is capable of simulating the plenum airflow pattern, temperature, velocity, heat flux, and total heat transfer with acceptable accuracy.

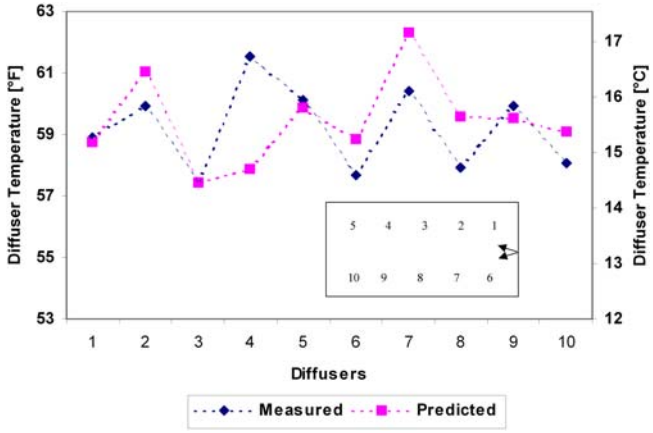

Figure 11 *Comparison of measured and CFD-predicted diffuser temperatures for the inlet vanes/two jets inlet configuration.*

For the given plenum shape, the major findings are as follows.

- The recirculation is larger in size with one inlet jet than with two jets.
- The temperature nonuniformity is greater with one inlet jet than with two jets.
- Air velocity in the plenum is generally low for both inlet configurations, compared with the inlet velocity. The resistance of the pedestals may not be ignored.
- The magnitude of the heat flux from the slab into the plenum is associated with the air velocity and air temperature, since convective heat transfer is a product of convective coefficient and temperature difference. Airflow has its highest velocity and lowest temperature at the plenum inlet. Obviously, the heat flux decreases gradually after the airflow enters the plenum.

SENSITIVITY STUDY USING THE VALIDATED MODEL

The validated CFD model can be used to investigate the impact of the design parameters, such as those associated with the inlet configurations on the plenum heat gain and temperature distribution. Some initial work has been accomplished and is presented in Table 3. A schematic diagram of the dimensions of the 20,000 ft^2 (1,860 m^2), 1 ft (0.3 m) high plenum under investigation (representing the floor plate of a building) and the locations of the inlets and the inlet airflow directions are shown in Figure 12. For the sake of brevity, internal and external inlets are shown together in the same figure. For these simulations, there were 60 diffusers total, 28 in the perimeter zone and 32 in the interior zone. For the sake of brevity, the diagram of the boundary conditions established for the sensi-

Table 1. Comparison of the Temperature Rise and Standard Deviation for Different Inlet Configurations

	One Jet	Two Jets
Supply temperature, °C (°F)	13.3 (56.0)	12.0 (53.6)
Average diffuser temperature, °C (°F)	17.0 (62.6)	15.1 (59.2)
Standard deviation for the diffuser temperatures, °C (°F)	1.6 (2.9)	0.8 (1.4)

Table 2. Comparison of Heat Gain into the Plenum Between Test and CFD Prediction

	One Jet		Two Jets	
	Measured, W (Btu/h)	Predicted, W (Btu/h)	Measured, W (Btu/h)	Predicted, W (Btu/h)
Floor	N/A	1322 (4510)	N/A	1612 (5500)
Slab	N/A	1753 (5981)	N/A	1379 (4705)
Total	3305 (11276)	3075 (10491)	2851 (9727)	2991 (10205)

Table 3. Plenum Heat Gain and Diffuser Temperature Distribution under Different Inlet Configurations

Case	Description	Inlet Velocity, ft/min (m/s)	Heat Gain, Btu/h·ft^2 (W/m^2)	Average Perimeter Temp, °F (°C)	Average Interior Temp, °F (°C)	Max/Min Perimeter Temp, °F (°C)	Max/Min Interior Temp, °F (°C)
1	Internal inlets low velocity	97.2 (0.49)	4.8 (15.2)	69.0 (20.6)	64.4 (18.0)	72.4/66.1 (22.5/19.0)	67.2/62.7 (19.6/17.0)
2	Internal inlets 600 fpm	600 (3.0)	5.0 (15.9)	65.4 (18.6)	68.1 (20.1)	67.2/63.5 (19.5/17.5)	72.8/62.9 (22.7/17.1)
3	Internal inlets 1,200 fpm	1,200 (6.1)	5.3 (16.6)	66.8 (19.3)	67.3 (19.6)	69.4/64.7 (20.8/18.2)	71.5/63.4 (21.9/17.5)
4	External inlets low velocity	33.4 (0.17)	4.2 (13.4)	63.6 (17.6)	68.0 (20.0)	63.8/63.3 (17.7/17.4)	71.4/66.0 (21.9/18.9)
5	External inlets small angle	1,200 (6.1)	5.5 (17.4)	66.8 (19.3)	67.7 (19.8)	71.5/63.2 (21.9/17.3)	69.8/64.6 (21.0/18.1)
6	External inlets large angle	1,200 (6.1)	5.9 (18.7)	67.8 (19.9)	66.9 (19.4)	69.4/65.7 (20.8/18.7)	68.4/63.9 (20.2/17.7)

tivity analysis cases presented in Table 3 is not shown; however, it is analogous to Figure 4. The boundary conditions are the same except for the inlet locations and air velocities. Specifically, the boundary conditions are: inlet air temperature, 62°F (16.7°C); airflow rate, 1 cfm/ft^2 (0.00508 m^3/s·m^2) or 20,000 cfm (9.44 m^3/s) total; ceiling temperature, 78°F (25.6°C); ceiling emissivity, 0.9; view factor, 0.5; and temperature under slab, 80°F (26.7°C). For the internal inlet cases, three inlet velocities varying from the theoretically lowest up to 1,200 ft/min (6.1 m/s) are investigated. As indicated, air is delivered into the plenum from each end of a simulated core region of the floor plate for the two higher inlet velocity cases. For the theoretically lowest inlet velocity case, it is assumed that air is supplied evenly along all edges of the simulated core region. Although it does not represent a realistic design, this case may be looked upon as a baseline where the minimum heat gain (lowest average velocities) could be achieved. For the external inlet cases, since direct shooting of the air into the interior zone is not good design practice, the analysis is based on how to turn the inlet jets toward the perimeter zone instead. The airflow is divided into four jets at each of the four inlet locations. The direction of each jet is defined by the angles α and β shown in Figure 12. Two cases are presented: α is 30° and β is 30° for case 5, and α is 30° and β is 45° for case 6. For the theoretically lowest inlet velocity case for the external inlet configuration, it is assumed that air is supplied evenly along all perimeter edges of the simulated plenum, producing an extremely low plenum inlet velocity (Table 3).

Table 3 shows that for all internal plenum inlet locations, the influence of the inlet velocity on the total plenum heat gain is small for the three cases studied. A net reduction of less than 10% was observed when velocities were reduced from 1,200 fpm (6.1 m/s) to the very low value near 100 fpm (0.5 m/s) (total volume remained the same). However, the uniformity of the temperature distribution in the interior and perimeter zones of the floor plate is influenced by the inlet velocities.

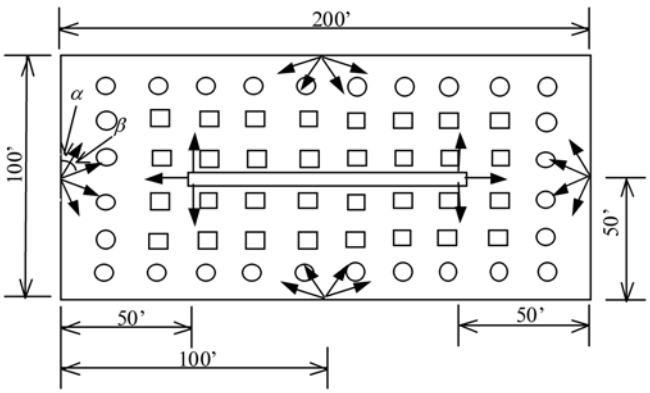

Figure 12 *Schematic of the inlet configurations for the internal and external inlets.*

Higher internal inlet velocities produce larger temperature variations in the interior zone, as some diffusers receive cool air directly from the incoming supply jet, while others receive warmer air that is recirculated back into the interior zone (Cases 2 and 3). In the case of the very low and evenly distributed internal inlet velocities (Case 1), plenum temperature variations in the interior zone are greatly reduced, but the perimeter zone experiences much higher temperatures.

For the external plenum inlet locations, the directions of the inlet jets affect the temperature distribution to some extent. Case 5, with smaller angles directing most of the supply air into the perimeter zone, produces a cooler average perimeter temperature but greater variability. Case 6 directs some air into the perimeter and some toward the interior, thereby producing greater overall uniformity. In the limit when extremely low inlet velocities along the perimeter edge are employed (Case 4), a significant reduction in the overall heat gain into the plenum is observed.

CONCLUSIONS

A CFD model for the underfloor supply plenum of a UFAD system was developed. The model can be used to predict the airflow patterns, air temperature and velocity distributions, and heat flux from the structural slab and the raised floor into the plenum for a variety of thermal and airflow boundary conditions. The model was validated using experimental data collected in a full-scale plenum test facility. The computed air temperature, velocity, and heat flux generally agree well with the measured data. More importantly, the discrepancies between computed and measured total heat gain of the plenum are less than 10%.

The CFD plenum model developed in this research is readily extendable to other plenum configurations. As an example of the use of the validated CFD model to investigate the impact of plenum inlet location and conditions, a series of sensitivity simulations using the validated CFD model was conducted. The sensitivity analysis demonstrated that inlet location, direction, and velocity may influence the temperature distribution in perimeter and interior zones of the building. Research is now under way to apply the CFD plenum model to a wider range of realistic underfloor air supply plenum configurations with the goal of providing design and operating guidelines.

ACKNOWLEDGMENTS

This work was primarily supported by the Center for the Built Environment (CBE) at the University of California, Berkeley. CBE is an NSF/Industry/University Cooperative Research Center whose current sponsors are: Armstrong World Industries; Arup; California Department of General Services; California Energy Commission; Charles Salter Associates, Inc.; Flack + Kurtz, Inc.; HOK; Pacific Gas & Electric Co.; Price Industries; RTKL Associates, Inc.; SOM; Steelcase, Inc.; Stantec; Syska Hennessy Group; Tate Access Floors, Inc.; the Taylor Team (Taylor Engineering, Engineering Enterprise, Guttmann & Blaevoet, Southland Industries, and the Swinerton Builders); Trane; US Department of Energy; US General Services Administration; Webcor Builders; York International; and the Regents of the University of California. Additional support was provided by the National Science Foundation (NSF) under Grant No. EEC-0225093. Partial support was provided by the California Energy Commission (CEC) Public Interest Energy Research (PIER) Buildings Program under Contract 500-01-035.

REFERENCES

Bauman, F. 2003. *Underfloor Air Distribution (UFAD) Design Guide*. Atlanta: American Society of Heating, Refrigerating and Air-Conditioning Engineers, Inc.

Bauman, F., H. Jin, and T. Webster. 2006. Heat transfer pathways in underfloor air distribution (UFAD) systems. *ASHRAE Transactions* 112(2).

CBE. 2005. Underfloor Air Technology Web site, http://www.cbe.berkeley.edu/underfloorair. Center for the Built Environment (CBE), University of California, Berkeley, CA.

Fujita, H., and S. Tomiie. 1999. Thermal storage with concrete slab of pressurized plenum in underfloor air distribution system. *Proceedings of Building Simulation '99, Kyoto, Japan, September 13–15* 1:499–506.

Launder, B.E., and D.B. Spalding. 1974. The numerical computation of turbulent flows. *Computer Methods in Applied Mechanics and Energy* 3:269–89.

Nagase, O., K. Matsunawa, H. Izuka, S.-I. Tanabe, and T. Arai. 1995. Effects of internal load, supply air volume, and floor surface conditions on the thermal environment in the office space with underfloor HVAC. *Proceedings, Annual Conference of the Society of Heating, Air-Conditioning, and Sanitary Engineers of Japan, Hiroshima, Japan, October 2–4*.

Webster, T., F. Bauman, and J. Reese. 2002. Underfloor air distribution: Thermal stratification. *ASHRAE Journal* 44(5):28–33.